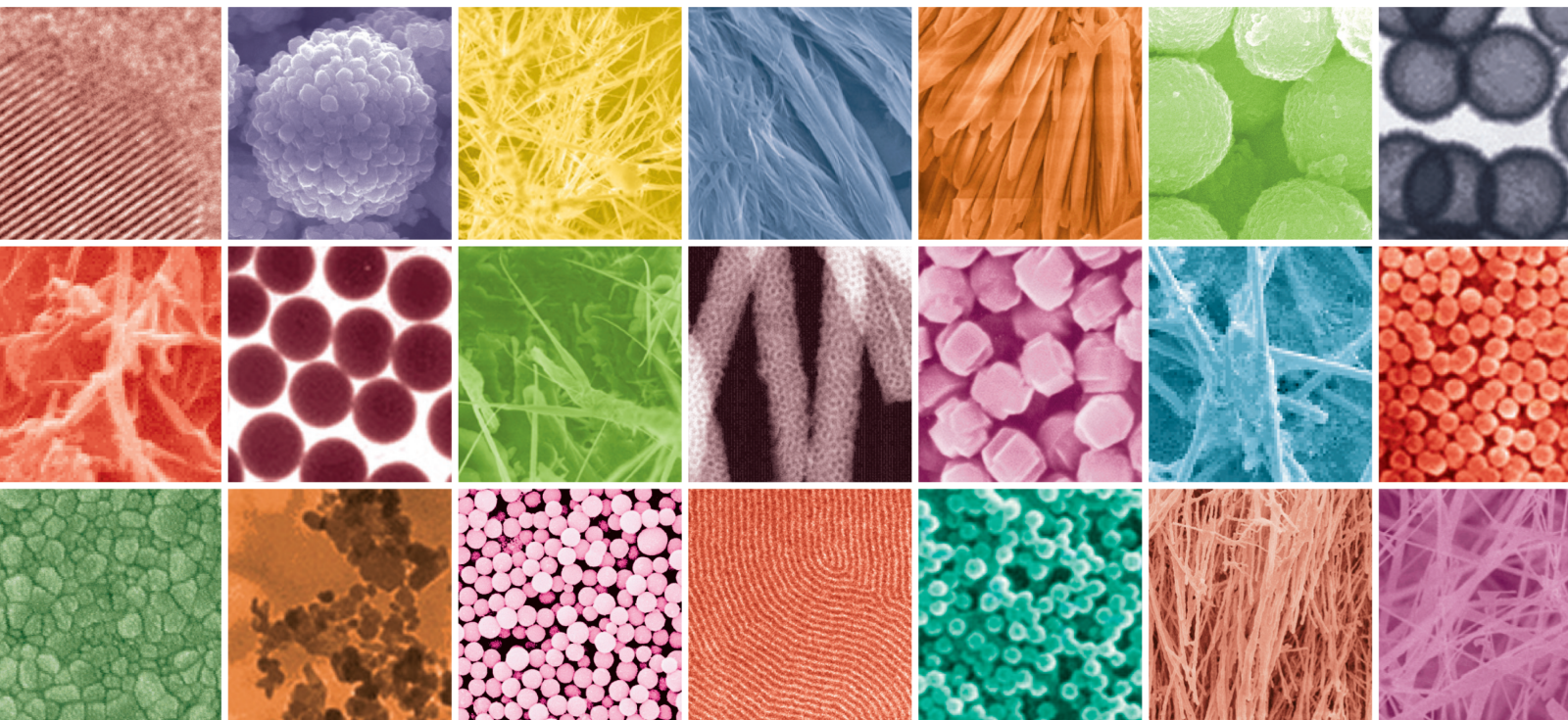


# Low-Dimensional Nanomaterials for Chemical Sensing, Energy and Photonics

Lead Guest Editor: Hao Xu

Guest Editors: Jiang Wu, Xiaoyu Han, and Qimiao Chen





---

# **Low-Dimensional Nanomaterials for Chemical Sensing, Energy and Photonics**

Journal of Nanomaterials

---

**Low-Dimensional Nanomaterials for  
Chemical Sensing, Energy and Photonics**

Lead Guest Editor: Hao Xu

Guest Editors: Jiang Wu, Xiaoyu Han, and Qimiao  
Chen



---




Copyright © 2020 Hindawi Limited. All rights reserved.

This is a special issue published in "Journal of Nanomaterials." All articles are open access articles distributed under the Creative Commons Attribution License, which permits unrestricted use, distribution, and reproduction in any medium, provided the original work is properly cited.


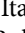

# Chief Editor

Stefano Bellucci , Italy

















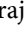
















## Associate Editors

Ilaria Armentano, Italy  
Stefano Bellucci , Italy  
Paulo Cesar Morais , Brazil  
William Yu , USA

## Academic Editors

Buzuayehu Abebe, Ethiopia  
Domenico Acierno , Italy  
Sergio-Miguel Acuña-Nelson , Chile  
Katerina Aifantis, USA  
Omer Alawi , Malaysia  
Nageh K. Allam , USA  
Muhammad Wahab Amjad , USA  
Martin Andersson, Sweden  
Hassan Azzazy , Egypt  
Ümit Ağbulut , Turkey  
Vincenzo Baglio , Italy  
Lavinia Balan , France  
Nasser Barakat , Egypt  
Thierry Baron , France  
Carlos Gregorio Barreras-Urbina, Mexico  
Andrew R. Barron , USA  
Enrico Bergamaschi , Italy  
Sergio Bietti , Italy  
Raghvendra A. Bohara, India  
Mohamed Bououdina , Saudi Arabia  
Victor M. Castaño , Mexico  
Albano Cavaleiro , Portugal  
Kondareddy Cherukula , USA  
Shafiul Chowdhury, USA  
Yu-Lun Chueh , Taiwan  
Elisabetta Comini , Italy  
David Cornu, France  
Miguel A. Correa-Duarte , Spain  
P. Davide Cozzoli , Italy  
Anuja Datta , India  
Loretta L. Del Mercato, Italy  
Yong Ding , USA  
Kaliannan Durairaj , Republic of Korea  
Ana Espinosa , France  
Claude Estournès , France  
Giuliana Faggio , Italy  
Andrea Falqui , Saudi Arabia

Matteo Ferroni , Italy  
Chong Leong Gan , Taiwan  
Siddhartha Ghosh, Singapore  
Filippo Giubileo , Italy  
Iaroslav Gnilitzkiy, Ukraine  
Hassanien Gomaa , Egypt  
Fabien Grasset , Japan  
Jean M. Greneche, France  
Kimberly Hamad-Schifferli, USA  
Simo-Pekka Hannula, Finland  
Michael Harris , USA  
Hadi Hashemi Gahruei , Iran  
Yasuhiko Hayashi , Japan  
Michael Z. Hu , USA  
Zhengwei Huang , China  
Zafar Iqbal, USA  
Balachandran Jeyadevan , Japan  
Xin Ju , China  
Antonios Kellarakis , United Kingdom  
Mohan Kumar Kesarla Kesarla , Mexico  
Ali Khorsand Zak , Iran  
Avvaru Praveen Kumar , Ethiopia  
Prashant Kumar , United Kingdom  
Jui-Yang Lai , Taiwan  
Saravanan Lakshmanan, India  
Meiyong Liao , Japan  
Shijun Liao , China  
Silvia Licoccia , Italy  
Zainovia Lockman, Malaysia  
Jim Low , Australia  
Rajesh Kumar Manavalan , Russia  
Yingji Mao , China  
Ivan Marri , Italy  
Laura Martinez Maestro , United Kingdom  
Sanjay R. Mathur, Germany  
Tony McNally, United Kingdom  
Pier Gianni Medaglia , Italy  
Paul Munroe, Australia  
Jae-Min Myoung, Republic of Korea  
Rajesh R. Naik, USA  
Albert Nasibulin , Russia  
Ngoc Thinh Nguyen , Vietnam  
Hai Nguyen Tran , Vietnam  
Hiromasa Nishikiori , Japan

Sherine Obare , USA  
Abdelwahab Omri , Canada  
Dillip K. Panda, USA  
Sakthivel Pandurengan , India  
Dr. Asisa Kumar Panigrahy, India  
Mazeyar Parvinzadeh Gashti , Canada  
Edward A. Payzant , USA  
Alessandro Pegoretti , Italy  
Oscar Perales-Pérez, Puerto Rico  
Anand Babu Perumal , China  
Suresh Perumal , India  
Thathan Premkumar , Republic of Korea  
Helena Prima-García, Spain  
Alexander Pyatenko, Japan  
Xiaoliang Qi , China  
Haisheng Qian , China  
Baskaran Rangasamy , Zambia  
Soumyendu Roy , India  
Fedlu Kedir Sabir , Ethiopia  
Lucien Saviot , France  
Shu Seki , Japan  
Senthil Kumaran Selvaraj , India  
Donglu Shi , USA  
Muhammad Hussnain Siddique , Pakistan  
Bhanu P. Singh , India  
Jagpreet Singh , India  
Jagpreet Singh, India  
Surinder Singh, USA  
Thangjam Ibomcha Singh , Republic of Korea  
Korea  
Vidya Nand Singh, India  
Vladimir Sivakov, Germany  
Tushar Sonar, Russia  
Pingan Song , Australia  
Adolfo Speghini , Italy  
Kishore Sridharan , India  
Marinella Striccoli , Italy  
Andreas Stylianou , Cyprus  
Fengqiang Sun , China  
Ashok K. Sundramoorthy , India  
Bo Tan, Canada  
Leander Tapfer , Italy  
Dr. T. Sathish Thanikodi , India  
Arun Thirumurugan , Chile  
Roshan Thotagamuge , Sri Lanka

Valeri P. Tolstoy , Russia  
Muhammet S. Toprak , Sweden  
Achim Trampert, Germany  
Tamer Uyar , USA  
Cristian Vacacela Gomez , Ecuador  
Luca Valentini, Italy  
Viet Van Pham , Vietnam  
Antonio Vassallo , Italy  
Ester Vazquez , Spain  
Ajayan Vinu, Australia  
Ruibing Wang , Macau  
Magnus Willander , Sweden  
Guosong Wu, China  
Ping Xiao, United Kingdom  
Zhi Li Xiao , USA  
Yingchao Yang , USA  
Hui Yao , China  
Dong Kee Yi , Republic of Korea  
Jianbo Yin , China  
Hesham MH Zakaly , Russia  
Michele Zappalorto , Italy  
Mauro Zarrelli , Italy  
Osman Ahmed Zeleke, Ethiopia  
Wenhui Zeng , USA  
Renyun Zhang , Sweden

## Contents

---

**Effects of Alumina Films on N-Doped Carbon Nanotubes/Graphene Composites as Anode Materials of Lithium-Ion Batteries**

Chuen-Chang Lin , Shu-Pei Hsu, and Guang-Jhong Chen

Research Article (13 pages), Article ID 6690401, Volume 2020 (2020)

## Research Article

# Effects of Alumina Films on N-Doped Carbon Nanotubes/Graphene Composites as Anode Materials of Lithium-Ion Batteries

Chuen-Chang Lin , Shu-Pei Hsu, and Guang-Jhong Chen

Department of Chemical & Materials Engineering, National Yunlin University of Science and Technology, 123 University Road Sec. 3, Douliu, Yunlin 64002, Taiwan

Correspondence should be addressed to Chuen-Chang Lin; [linchuen@yuntech.edu.tw](mailto:linchuen@yuntech.edu.tw)

Received 27 October 2020; Revised 10 November 2020; Accepted 13 November 2020; Published 29 November 2020

Academic Editor: Xiaoyu Han

Copyright © 2020 Chuen-Chang Lin et al. This is an open access article distributed under the Creative Commons Attribution License, which permits unrestricted use, distribution, and reproduction in any medium, provided the original work is properly cited.

A carbon nanotubes/graphene composite is grown on nickel foil without additional catalysts by one-step ambient pressure chemical vapor deposition (CVD). Next, the carbon nanotubes/graphene composite is modified by radio frequency (RF) nitrogen plasma. Finally, to improve its initial coulombic efficiency/electrochemical stability, lower potential during the charge process (coin cell), and boost potential during the discharge process (lithium-ion battery), alumina is deposited onto the N-doped carbon nanotubes/graphene composite by RF magnetron sputtering at different power levels and periods of time. The charge specific capacity (597 mAh/g) and initial coulombic efficiency (81.44% > 75.02% for N-doped carbon nanotubes/graphene) of Al<sub>2</sub>O<sub>3</sub>/N-doped CNTs/graphene for the coin cell reached a maximum at the best sputtering condition (power = 65 W and time = 30 min). Al<sub>2</sub>O<sub>3</sub>/N-doped CNTs/graphene (the best sputtering condition) exhibits higher initial coulombic efficiency (79.8%) compared with N-doped CNTs/graphene (initial coulombic efficiency: 74.3%) for the lithium-ion battery. Furthermore, the achievement fraction (about 70%) of full charge capacity (coin cell) for Al<sub>2</sub>O<sub>3</sub>/N-doped carbon nanotubes/graphene (the best sputtering condition) is higher than that (about 30%) for N-doped carbon nanotubes/graphene at a voltage lower than about 0.25 V. Moreover, it also shows a little higher electrochemical stability (coin cell) of charge capacity for Al<sub>2</sub>O<sub>3</sub>/N-doped carbon nanotubes/graphene (the best sputtering condition) in comparison with N-doped carbon nanotubes/graphene and Al<sub>2</sub>O<sub>3</sub>/N-doped CNTs/graphene (the best sputtering condition) exhibits better cyclic stability (lithium-ion battery) of discharge capacity compared with N-doped CNTs/graphene.

## 1. Introduction

The applications of lithium-ion batteries include portable electronic devices, electric vehicles, and hybrid electric vehicles. In comparison with other batteries, lithium-ion batteries have higher energy densities, higher voltage, and lower maintenance [1]. The performance of lithium-ion batteries mainly depends on the properties of anode and cathode materials. In this research, we focused on anode materials of lithium-ion batteries.

In our previous study [2], one-step ambient pressure CVD was used to simultaneously synthesize carbon nano-

tubes (CNTs) as well as graphene on nickel foam without additional catalysts at 800°C and then the carbon nanotubes/graphene composite was modified by RF nitrogen plasma treatment. However, it still possessed lower initial coulombic efficiency/electrochemical stability and mainly occurred higher potential during the charge process of the coin cell as well as lower potential during the discharge process of the lithium-ion battery for the N-doped carbon nanotubes/graphene composite. Therefore, to improve its initial coulombic efficiency/electrochemical stability, lower potential during the charge process of the coin cell, and enhance potential during the discharge process of the lithium-ion



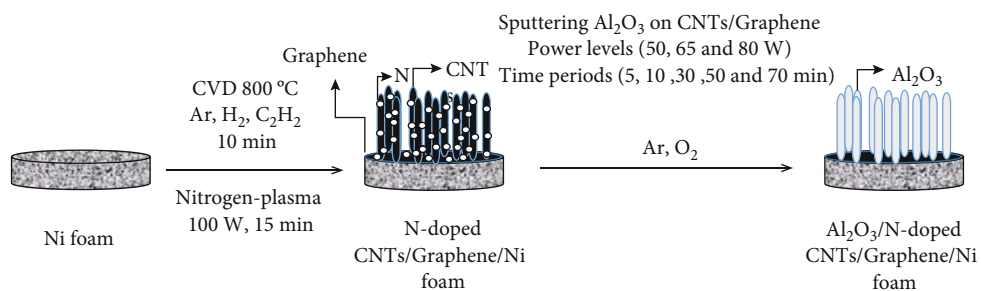


FIGURE 1: Schematic illustration of the fabrication process of Al<sub>2</sub>O<sub>3</sub>/N-doped CNTs/graphene.

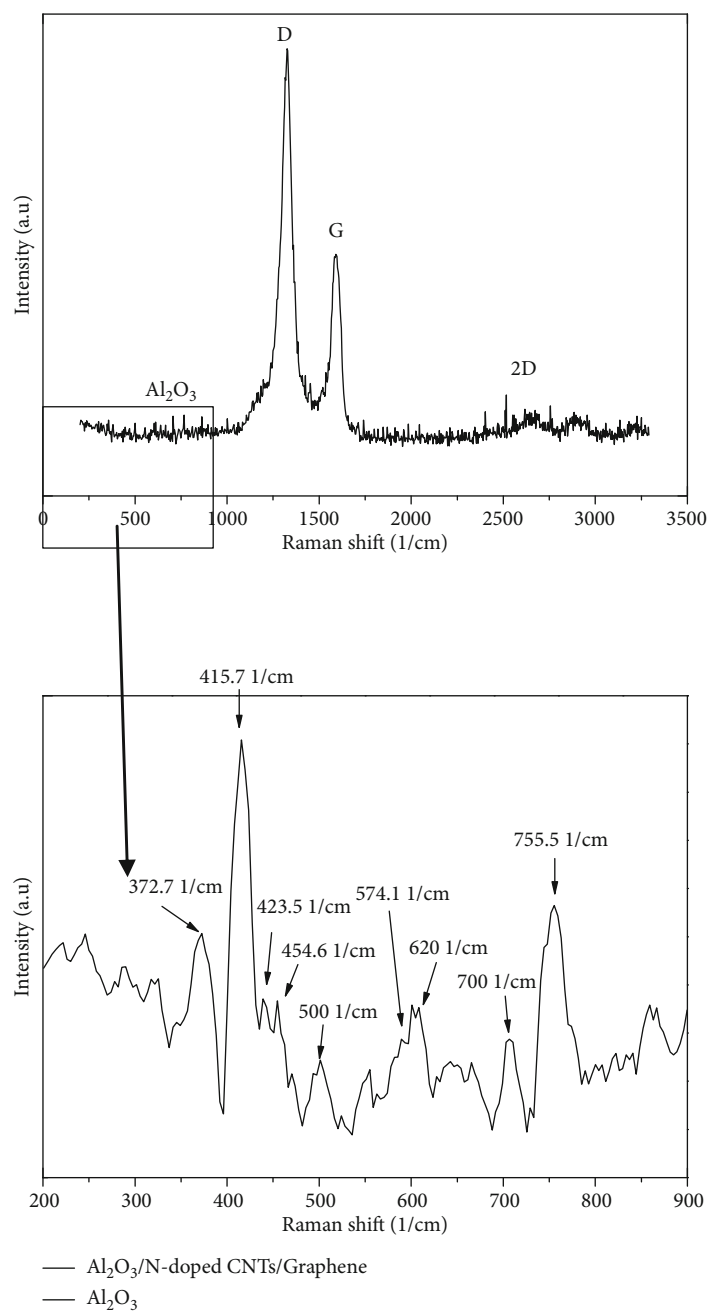


FIGURE 2: Raman spectra of Al<sub>2</sub>O<sub>3</sub>/N-doped CNTs/graphene.

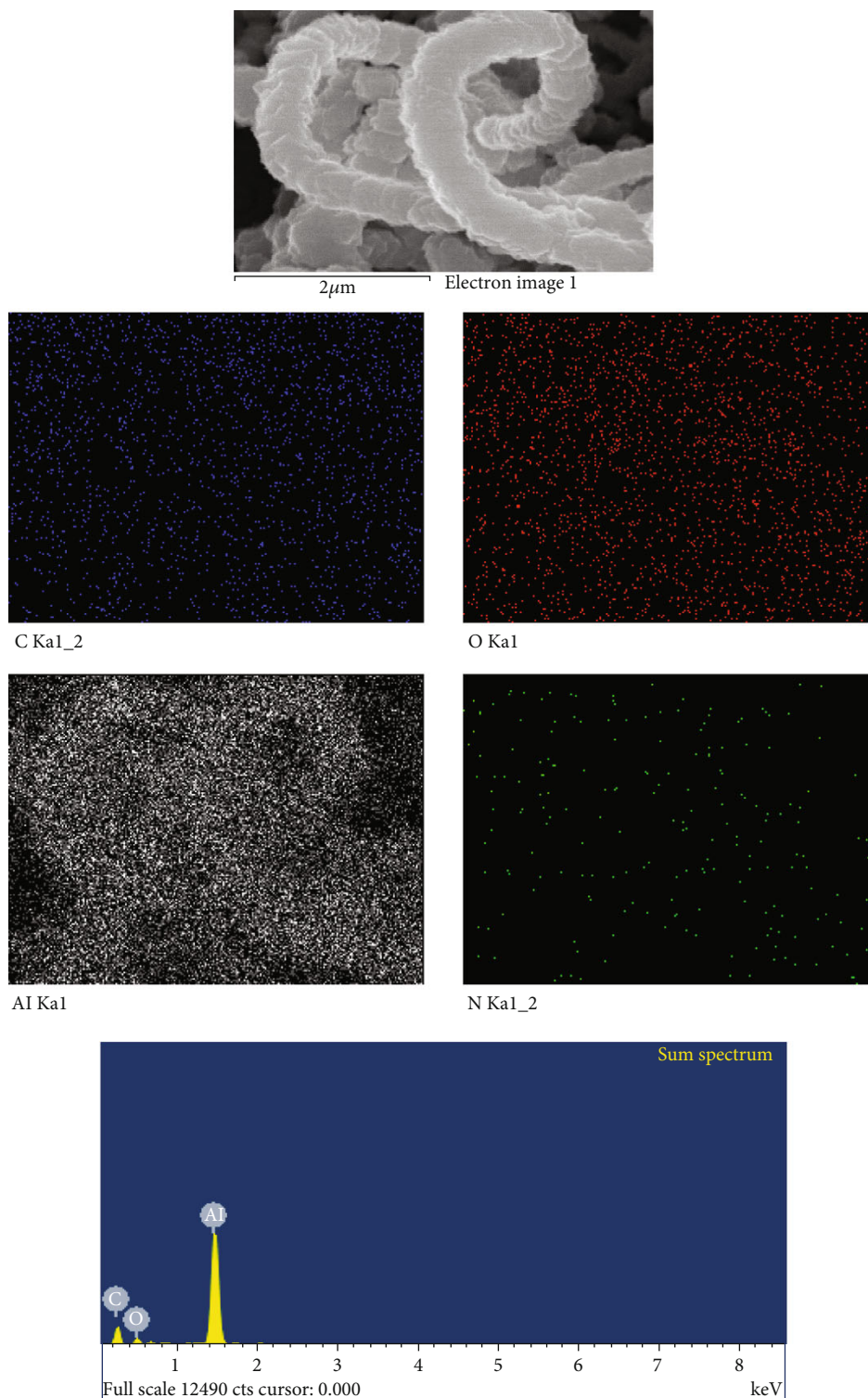


FIGURE 3: The FESEM image and EDX elemental mappings as well as intensities of C, O, Al, and N in  $Al_2O_3$ /N-doped CNTs/graphene (the best sputtering condition).

battery, the N-doped carbon nanotubes/graphene composite was modified by oxides in this research.

An alumina layer was deposited on silicon by atomic layer deposition (ALD) to prevent some side reactions between the silicon and the electrolyte, and then the

coulombic efficiency and electrochemical stability were improved [3]. A smooth alumina protective layer was deposited on Al-doped (enhancing the electronic conductivity of insulating alumina) porous C/SiO<sub>2</sub> composites, and alumina could act as a preformed solid electrolyte

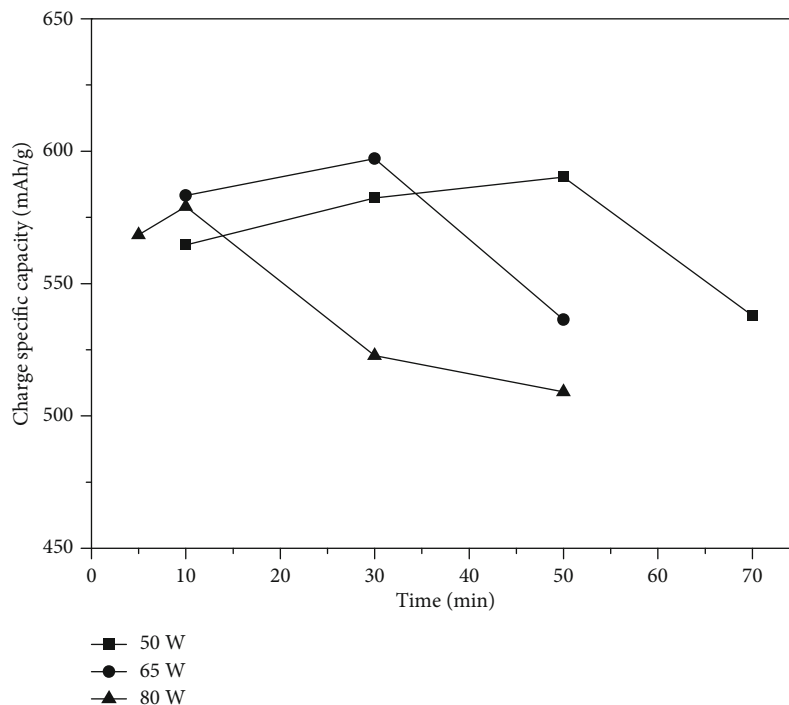


FIGURE 4: The effects of power levels and time periods for sputtering alumina onto N-doped carbon nanotubes/graphene composites on the charge specific capacity (0.1 C) of alumina/N-doped carbon nanotubes/graphene for the coin cell.

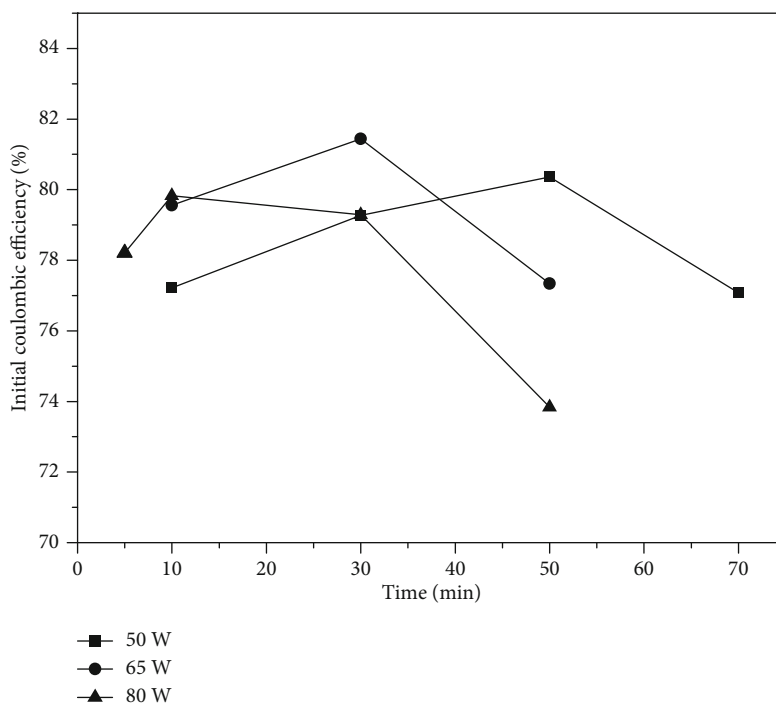


FIGURE 5: The effects of power levels and time periods for sputtering alumina onto N-doped carbon nanotubes/graphene composites on the initial coulombic efficiency of alumina/N-doped carbon nanotubes/graphene for the coin cell.

interface (SEI) film to decrease lithium ions consumption in the regeneration of SEI films as well as then increase the coulombic efficiency as well as electrochemical stability

[4]. Alumina artificial SEI layers with different thickness which suppressed the growth of SEI films were deposited on the  $\text{SnO}_2/\text{CNTs}$  composite by ALD at different cycles,

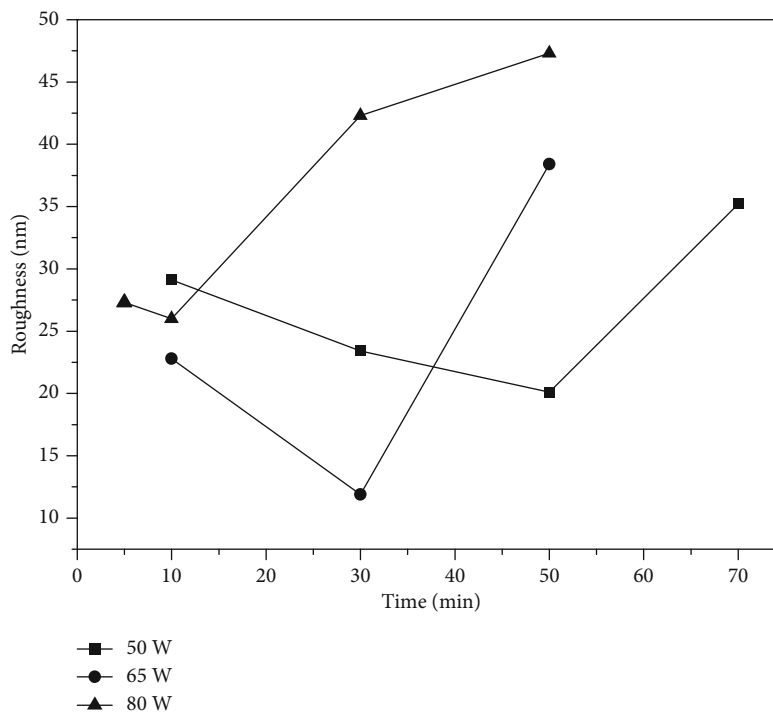


FIGURE 6: The effects of power levels and time periods for sputtering alumina onto N-doped carbon nanotubes/graphene composites on the roughness of alumina/N-doped carbon nanotubes/graphene.

and electrochemical stability, rate capability, and coulombic efficiency were improved [5]. An alumina passive layer which blocked the interaction between  $\text{Fe}_3\text{O}_4$  and the electrolyte to prevent the formation of SEI films was deposited on  $\text{Fe}_3\text{O}_4$ -reduced graphene oxide composite by ALD, and electrochemical stability was improved [6]. Alumina coating was deposited on the  $\text{MnO}_2/\text{CNTs}$  composites by ALD, and the initial coulombic efficiency was increased with the increase of the coating thickness; however, a thick alumina film decreased the electrochemical performances by inhibiting lithium-ion intercalation [7]. To improve the initial coulombic efficiency, electrochemical stability, and high-rate performance, alumina was coated on natural graphite powder by a sol-gel method and the alumina coating could act as a preformed SEI film to allow lithium-ion transport, prevent electron transfer, and reduce the regeneration of SEI films as well as lithium ion consumption during subsequent cycling [8]. Multi-walled carbon nanotubes (MWCNTs) were directly grown on the Cu current collector by CVD, then alumina was deposited on the MWCNTs by ALD, and alumina could enhance electrochemical stability and lithium-ion intercalation capacity [9]. Alumina with different thickness was deposited on lithium metal by RF magnetron sputtering at a fixed power level (80 W) as well as different time periods (10 min-60 min), and lithium metal coated with a 20 nm thick alumina possessed better electrochemical stability than lithium metal [10]. So, alumina was deposited onto the N-doped carbon nanotubes/graphene composite by RF magnetron sputtering at different power levels and periods of time in this study.

## 2. Materials and Methods

We followed the methods of Lin et al. (2018) [11] and Lin et al. (2020) [12] to prepare a carbon nanotubes/graphene composite. Next, the carbon nanotubes/graphene composite was modified by nitrogen plasma according to the method of Lin et al. (2020) [12]. Finally, alumina was deposited onto the N-doped carbon nanotubes/graphene composite by RF magnetron sputtering from a 3 inch disk Al target (purity: 99.7%, purchased from Solar Applied Materials Technology Corporation, Taiwan) in a vacuum chamber with a background pressure of  $7 \times 10^{-6}$  torr. The distance between the target and the substrate was 8 cm. The pressure and volume flow rates of argon as well as oxygen were maintained at 20 mtorr and 25 sccm as well as 10 sccm, respectively. The power levels (50, 65, and 80 W) and time periods (5, 10, 30, 50, and 70 min) were varied.

A solution of 1 M  $\text{LiPF}_6$  dissolved in 1:1:1 (wt%) ethylene carbonate-ethyl methyl carbonate-dimethyl carbonate from Ubiq Technology was used as the electrolyte. The anode electrode ( $\pi \times 0.65 \times 0.65 \text{ cm}^2$ , Li metal: 99.9%, 0.3 mm thick, Ubiq Technology) was assembled with the cathode electrode ( $\pi \times 0.65 \times 0.65 \text{ cm}^2$ , N-doped CNTs/graphene or  $\text{Al}_2\text{O}_3/\text{N-doped CNTs/graphene}$ ) into a coin cell with the 0.1-0.15 ml electrolyte (1 M  $\text{LiPF}_6$ ) and the PP/PE/PP separator (Celgard 2325, Celgard, USA) at room temperatures (about 293-303 K) by using a coin cell manual crimping machine (CR2032, Taiwan) in an Ar-filled glove box. Furthermore, the cathode electrode ( $\pi \times 0.65 \times 0.65 \text{ cm}^2$ ,  $\text{LiCoO}_2$ : 92% of purity, Ubiq Technology) was assembled with the anode electrode ( $\pi \times 0.65 \times 0.65 \text{ cm}^2$ ,  $\text{Al}_2\text{O}_3/\text{N}$ -

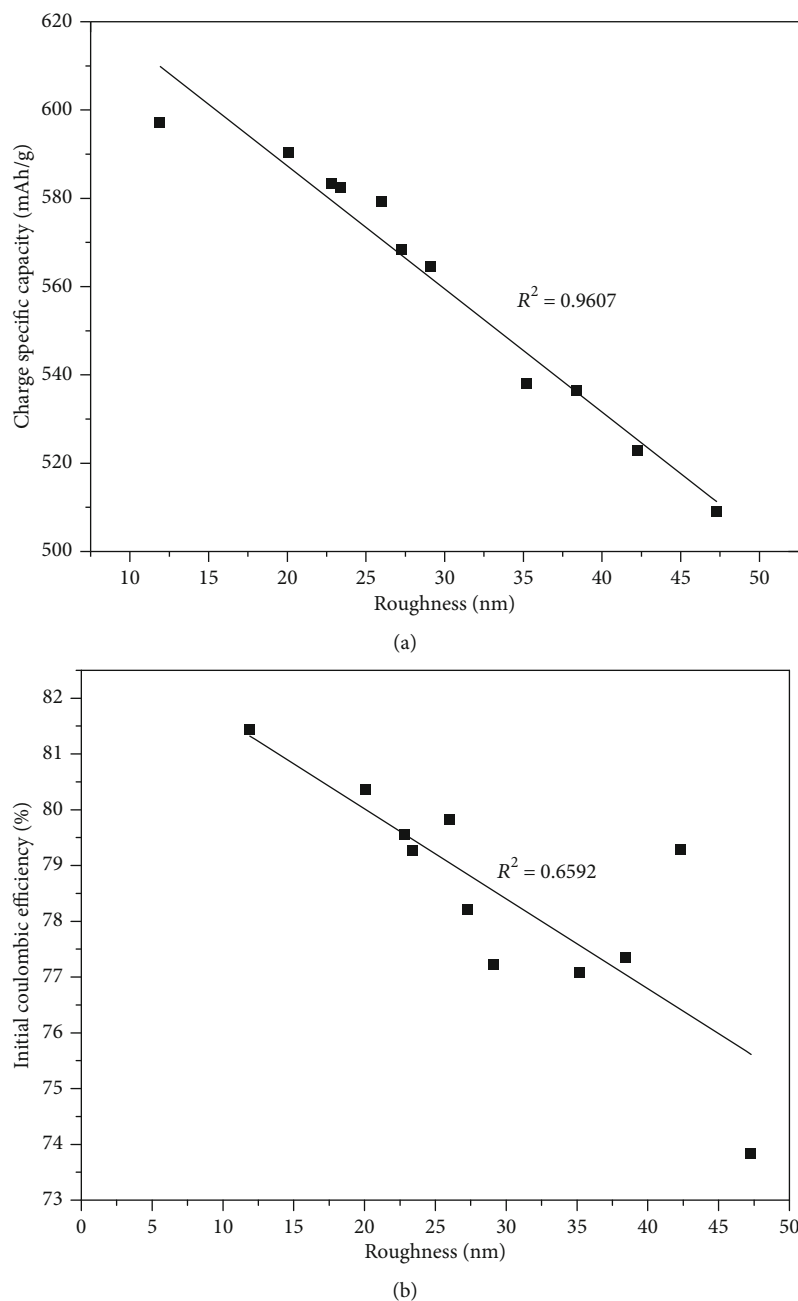


FIGURE 7: (a) The correlation between the charge specific capacity and the roughness and (b) the correlation between the initial coulombic efficiency and the roughness.

doped carbon nanotubes/graphene composites (the best sputtering condition)) into a lithium-ion battery (full cell) with the same procedure as the coin cell. The electrochemical cycling tests were performed at 0.1-2 C with a potential range of 0.01 V to 3 V (vs.  $\text{Li}^+/\text{Li}$ ) for the coin cell (a potential range of 1-4.5 V for the full cell) using a cyler (PFX 2011, Kikusui, Japan).

The D peak, G peak, 2D peak, and  $\text{Al}_2\text{O}_3$  peak for the  $\text{Al}_2\text{O}_3/\text{N}$ -doped carbon nanotubes/graphene composite (the best sputtering condition) were investigated by microscopic Raman spectrometer (633 nm of wavelength; in Via, Renishaw, England). Furthermore, the structure or chemical composition of  $\text{Al}_2\text{O}_3/\text{N}$ -doped CNTs/graphene

for sputtering alumina onto N-doped CNTs/graphene composites at 65 W and different time periods were conducted by field emission scanning electron microscope (FE-SEM) combined with energy-dispersive X-ray (EDX) (JEOL JSM-6700F, Japan). Additional information on the surface roughness (root-mean-square (rms) got by running NanoScope Analysis using original AFM data as input) of  $\text{Al}_2\text{O}_3/\text{N}$ -doped CNTs/graphene for sputtering alumina onto N-doped CNTs/graphene composites at different power levels and time periods was obtained by atomic force microscope (AFM, Dimension ICON Bruker, Germany). Moreover, cyclic voltammetry tests of the coil cell for  $\text{Al}_2\text{O}_3/\text{N}$ -doped CNTs/graphene (the best sputtering

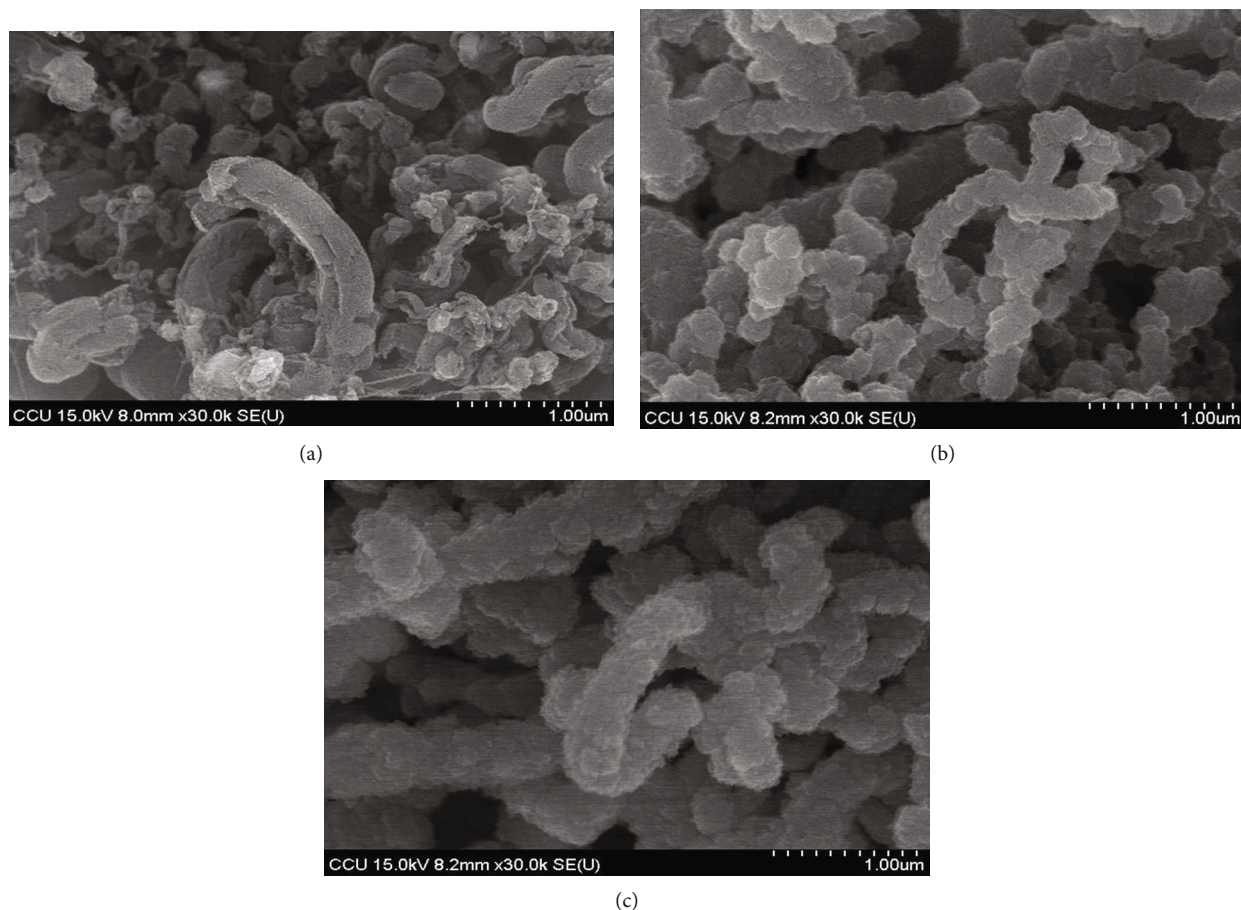


FIGURE 8: The FESEM images of  $\text{Al}_2\text{O}_3/\text{N}$ -doped CNTs/graphene with the power level (65 W) and different time periods (a) 10 min, (b) 30 min, and (c) 50 min for sputtering  $\text{Al}_2\text{O}_3$  onto N-doped CNTs/graphene composites.

condition) were performed using an electrochemical analyzer (CH Instruments CHI 608B, USA) with the CR2032 coin cell over a potential range of 0.01-3.0 V at a scan rate of  $0.1 \text{ mV s}^{-1}$ .

### 3. Results and Discussion

Figure 1 shows alumina fabricated by sputtering  $\text{Al}_2\text{O}_3$  onto the N-doped CNTs/graphene composite grown on nickel foam by CVD and treated with  $\text{N}_2$  plasma. The Raman spectra (see Figure 2) for the  $\text{Al}_2\text{O}_3/\text{N}$ -doped carbon nanotubes/graphene composite (the best sputtering condition), the peaks positioned at  $1350 \text{ cm}^{-1}$  (D),  $1550 \text{ cm}^{-1}$  (G), and  $2665 \text{ cm}^{-1}$  (2D), can be assigned to CNTs as well as graphene which also are confirmed by the FESEM images of CNTs as well as graphene sheets being simultaneously synthesized at  $800^\circ\text{C}$  in our previous paper [2]; the peaks located at  $372.7 \text{ 1/cm}$ ,  $415.7 \text{ 1/cm}$ ,  $423.5 \text{ 1/cm}$ ,  $454.6 \text{ 1/cm}$ ,  $574.1 \text{ 1/cm}$ , and  $755.5 \text{ 1/cm}$  corresponding to the  $E_g(\text{TO})$ ,  $A_{1g}(\text{LO})$ ,  $E_g(\text{TO})$ ,  $E_g(\text{LO})$ ,  $E_g(\text{LO})$ , and  $E_g(\text{LO})$ , respectively, can be attributed to  $\text{Al}_2\text{O}_3$  as well as are in good agreement with the previous literature [13], and the sharp peaks at about  $500 \text{ 1/cm}$  and  $700 \text{ 1/cm}$  are spinel  $\gamma\text{-Al}_2\text{O}_3$  as well as the sharp peak at about  $620 \text{ 1/cm}$  is nonspinel  $\gamma\text{-Al}_2\text{O}_3$  [14]. Furthermore, alu-

mina coated onto the N-doped CNTs/graphene composite was also verified from the EDX element mappings and intensities in Figure 3 which exhibited Al and O for  $\text{Al}_2\text{O}_3/\text{N}$ -doped CNTs/graphene.

Figures 4 and 5 show the effects of power levels and time periods for sputtering alumina onto N-doped carbon nanotubes/graphene composites on the charge specific capacity (0.1 C) and initial coulombic efficiency of alumina/N-doped carbon nanotubes/graphene for the coin cell, respectively. The charge specific capacity ( $597 \text{ mAh/g}$ ) and initial coulombic efficiency (81.44%) reached a maximum at the best sputtering condition (power = 65 W and time = 30 min). The higher the surface roughness, the lower the charge specific capacity (see Figures 4 and 6) and nearly the lower the initial coulombic efficiency (see Figures 5 and 6) since a higher rough surface leads to probably increasing electrolyte decomposition, then forming more SEI, and also consuming more lithium ions during pre-discharging [8]. They also show that the charge specific capacity is obviously proportional to the surface roughness ( $R^2 = 0.96$ ; see Figure 7(a)), and initial coulombic efficiency is nearly proportional to the surface roughness ( $R^2 = 0.66$ ; see Figure 7(b)). Furthermore, the charge specific capacity increased with time periods in the range 10-30 min for 65 W of the power level. This picture

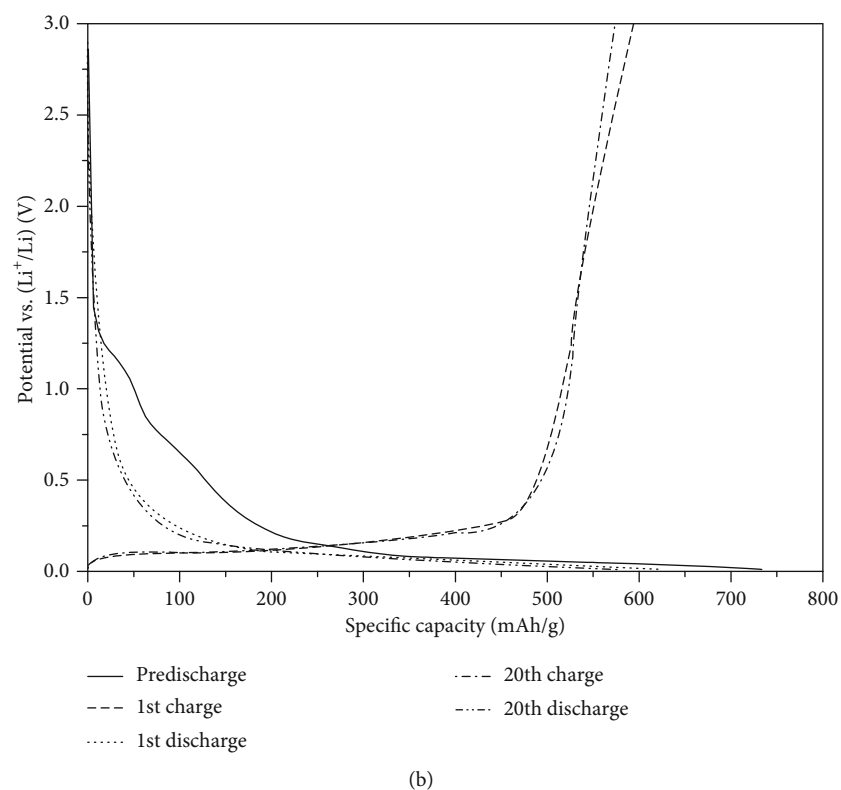
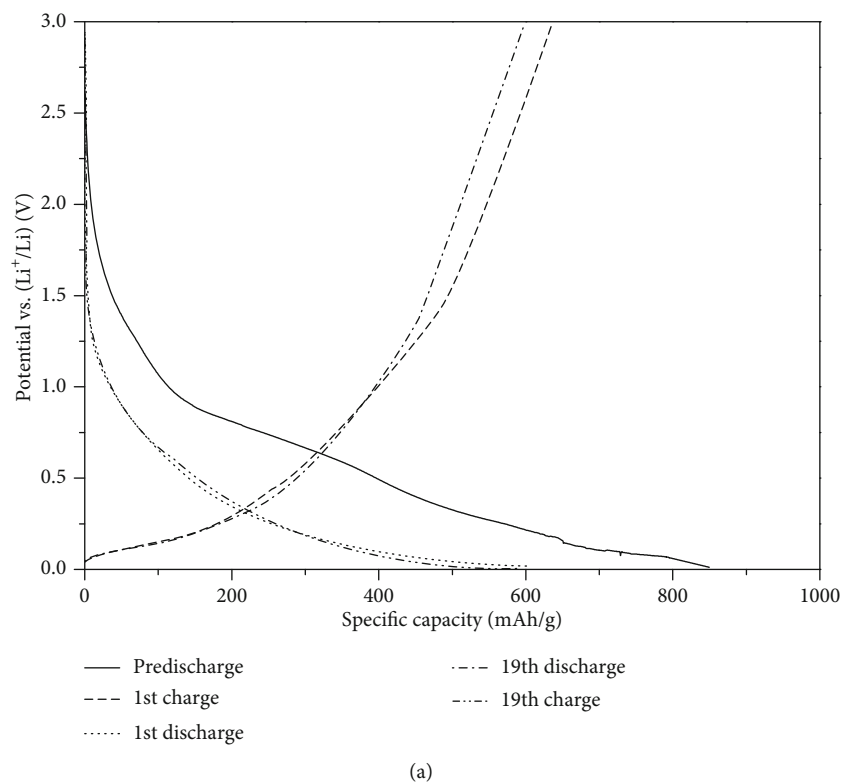
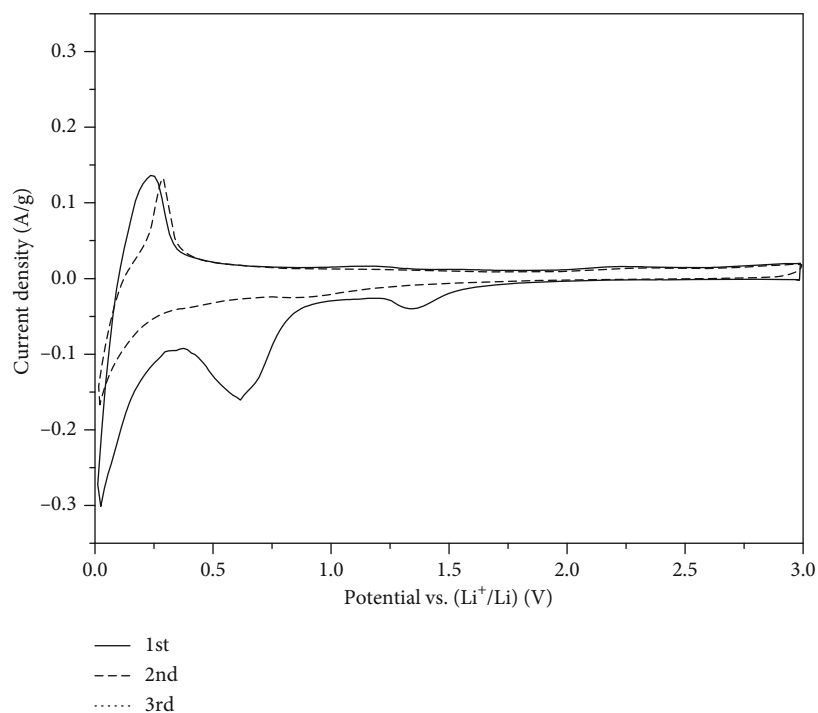


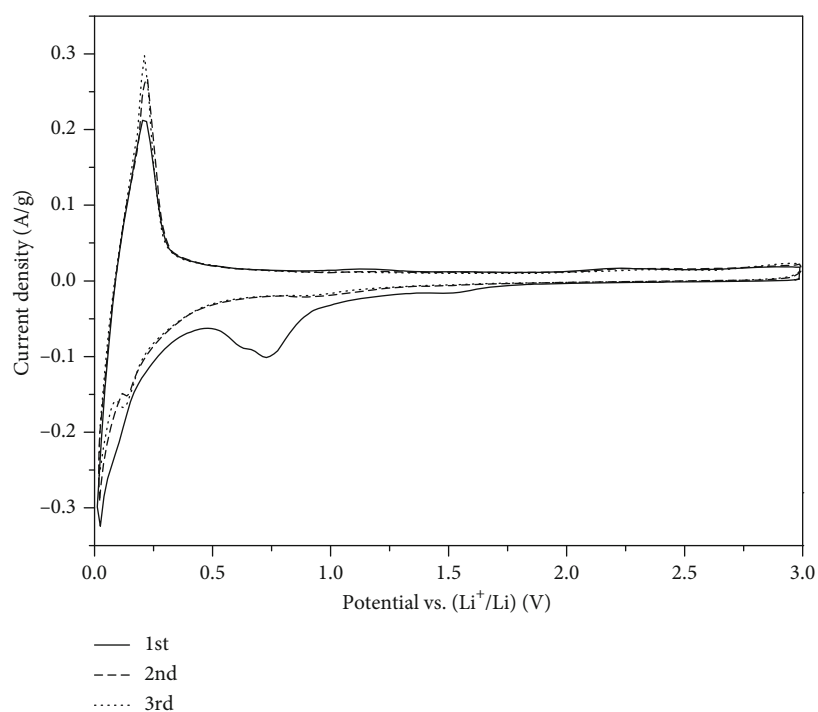
FIGURE 9: The discharge-charge profiles (between 0.01 V and 3 V at 0.1 C) with different charge-discharge cycles of the coin cell for (a) the N-doped CNTs/graphene composite [2] and (b)  $\text{Al}_2\text{O}_3/\text{N}$ -doped CNTs/graphene (the best sputtering condition).

may be explained as follows. A shorter time period (10 min) leads to less  $\text{Al}_2\text{O}_3$  deposited and forming a thinner  $\text{Al}_2\text{O}_3$  coating (see Figure 8(a)), which might not be insulating as

well as strong enough to act as a proper preformed SEI as well as reduce SEI formation during predischarging; then, charge specific capacity is lower (see Figure 4), and thus, initial



(a)



(b)

FIGURE 10: Cyclic voltammograms (between 0.01 V and 3 V from the 1st cycle to the 3rd cycle) of the coin cell for (a) the N-doped CNTs/graphene composite and (b)  $\text{Al}_2\text{O}_3/\text{N}$ -doped CNTs/graphene (the best sputtering condition).

coulombic efficiency is lower (see Figure 5). A longer time period (30 min) leads to more  $\text{Al}_2\text{O}_3$  homogeneously deposited and forming a uniform  $\text{Al}_2\text{O}_3$  coating layer with proper thickness (see Figure 8(b)) that could act as a preformed SEI to reduce SEI formation during pre-discharging; then, charge

specific capacity is higher (see Figure 4), and thus, initial coulombic efficiency is higher (see Figure 5). However, the charge specific capacity decreased with time periods in the range 30-50 min for 65 W of the power level. The reason behind this may be that an overly long time period leads to



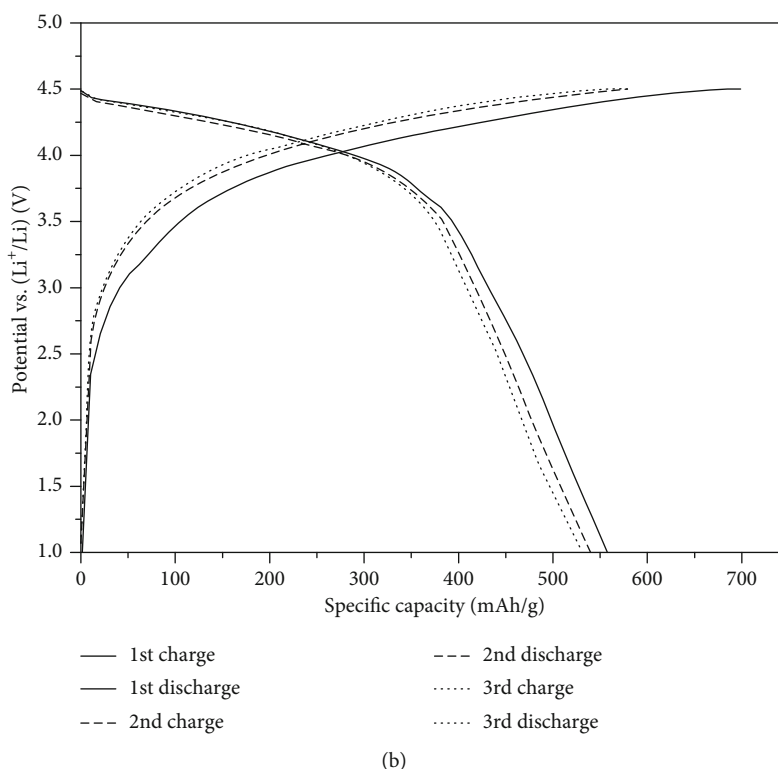
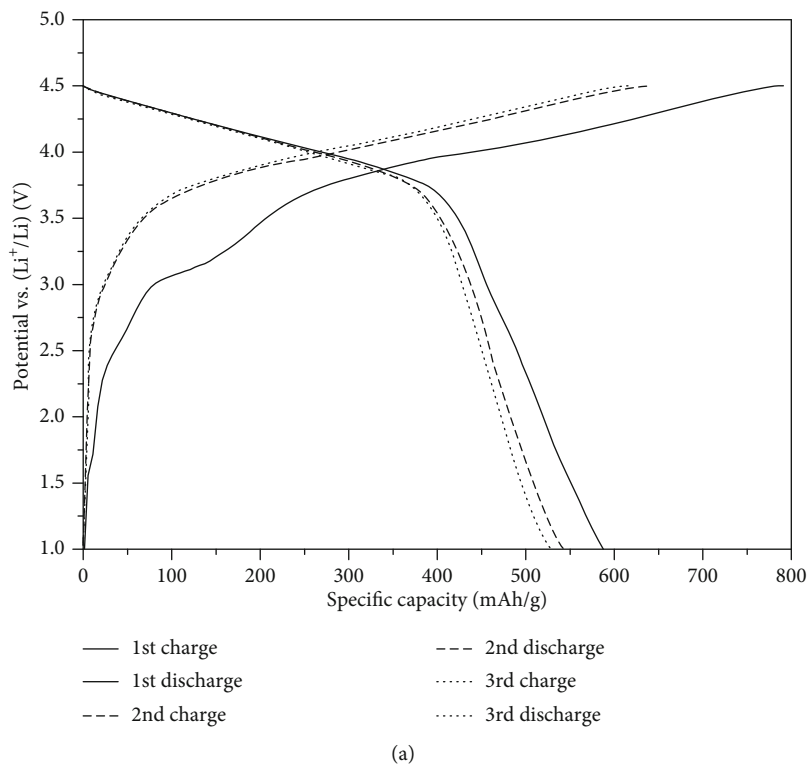


FIGURE 11: The discharge-charge profiles (between 1 V and 4.5 V at 0.1 C) with different charge-discharge cycles of the lithium-ion battery (full cell) for (a) the N-doped CNTs/graphene composite and (b)  $\text{Al}_2\text{O}_3/\text{N-doped CNTs/graphene}$  (the best sputtering condition).

an overly much  $\text{Al}_2\text{O}_3$  deposited and forming a  $\text{Al}_2\text{O}_3$  coating layer with over thickness (see Figure 8(c)), which could decrease lithium-ion to diffuse through it, then decreasing charge specific capacity (see Figure 4), and thus decreasing

initial coulombic efficiency (see Figure 5). The above behavior is similar to the previous literature [7].

Figures 9(a) and 9(b) show the discharge-charge profiles (0.1 C) of the coin cell for N-doped CNTs/graphene and

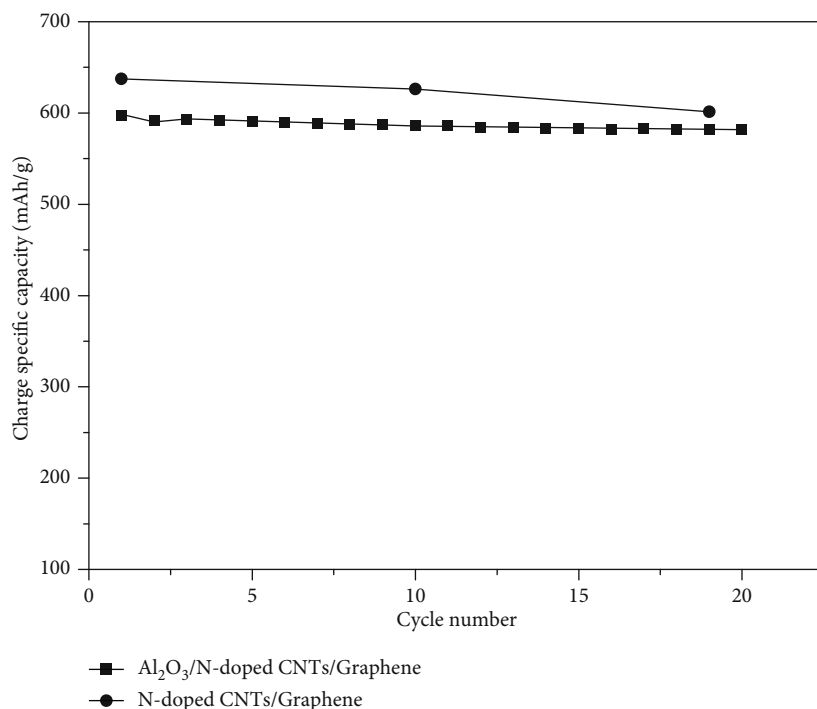


FIGURE 12: The effects of the N-doped CNTs/graphene composite [2], Al<sub>2</sub>O<sub>3</sub>/N-doped CNTs/graphene (the best sputtering condition), and different charge-discharge cycles on the charge specific capacity (0.1 C) for the coin cell.

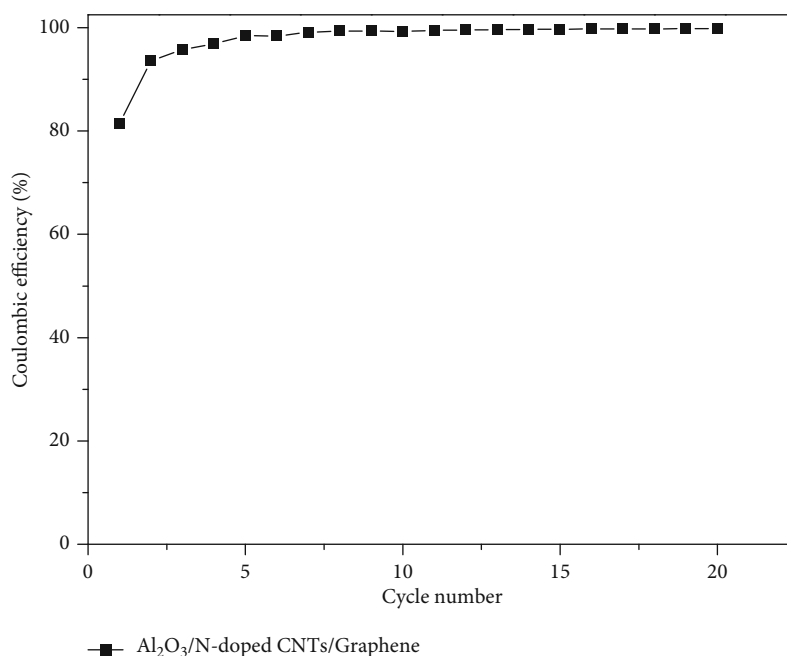


FIGURE 13: The effects of different charge-discharge cycles on the coulombic efficiency of Al<sub>2</sub>O<sub>3</sub>/N-doped CNTs/graphene (the best sputtering condition) for the coin cell.

Al<sub>2</sub>O<sub>3</sub>/N-doped CNTs/graphene (the best sputtering condition). The appearance of the plateaus in the predischage curve can be assigned to forming the SEI film on the surface of electrodes as well as the degrading electrolyte [15], and the predischage plateaus rapidly disappear in the following cycles (see Figures 9(a) and 9(b)) which also are verified by

the cathode peaks (about 0.6 V-0.7 V) happening during the 1st (predischage) cycle and disappearing in the subsequent cycles (see Figures 10(a) and 10(b)). The cathode peak (about 0.7 V) in the 1st (predischage) cycle of Al<sub>2</sub>O<sub>3</sub>/N-doped CNTs/graphene (the best sputtering condition) is not sharper than the cathode peak (about 0.6 V) in the 1st

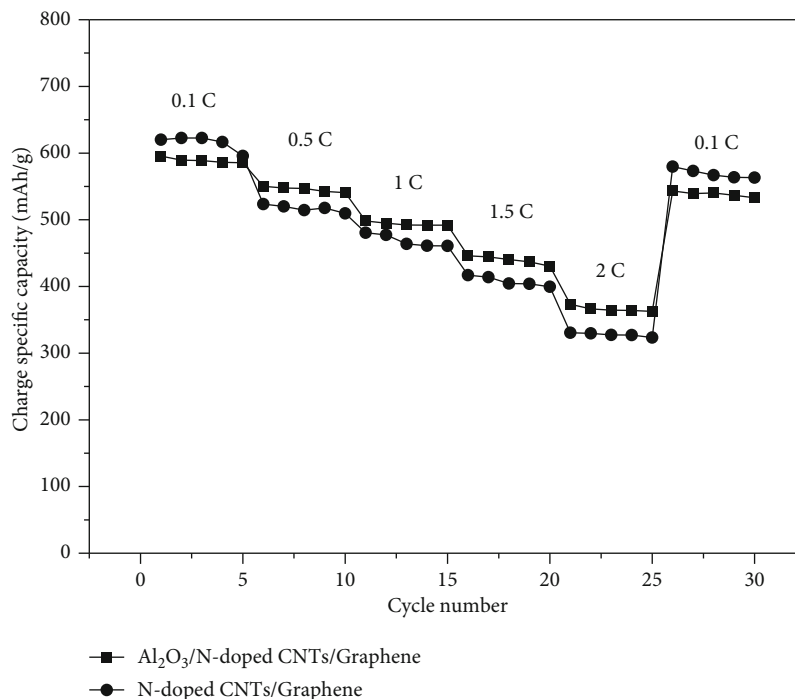


FIGURE 14: Rate capability (between 0.01 V and 3 V) with different charge-discharge cycles of the coin cell for the N-doped CNTs/graphene composite and Al<sub>2</sub>O<sub>3</sub>/N-doped CNTs/graphene (the best sputtering condition).

(predischarge) cycle of N-doped CNTs/graphene (see Figures 10(a) and 10(b)) since Al<sub>2</sub>O<sub>3</sub> coating layer could act as a preformed SEI to block the electrolyte, then suppress undesired side reactions with the electrolyte, and thus reduce SEI formation during predischarging. Therefore, the potential plateau in the predischarge curve of Al<sub>2</sub>O<sub>3</sub>/N-doped CNTs/graphene (the best sputtering condition) is not more obvious than that of N-doped CNTs/graphene and is extended over wider voltage ranges (about 1 V-0.5 V) that may be related to initial breakdown of the oxide [9]. Furthermore, an important feature of the discharge-charge profiles for Al<sub>2</sub>O<sub>3</sub>/N-doped CNTs/graphene (the best sputtering condition) is availability of the good fraction (about 70%) of full charge capacity at a voltage lower than about 0.25 V which is the potential plateau in the charge curves of Figure 9(b) that can be attributed to the Li<sup>+</sup> deintercalation from the carbon (see Figure 10(b)) [2]. However, the fraction (about 30%) of full charge capacity at a voltage lower than about 0.25 V for N-doped CNTs/graphene is bad (see Figure 9(b)). If charge specific capacity (about 400 mAh/g) is the same, it occurs at lower potential (about 0.25 V) for Al<sub>2</sub>O<sub>3</sub>/N-doped CNTs/graphene (the best sputtering condition) and at higher potential (about 1.1 V) for N-doped CNTs/graphene (see Figures 9(a) and 9(b)). Therefore, the cathode electrode (LiCoO<sub>2</sub>) was assembled with the anode electrode (Al<sub>2</sub>O<sub>3</sub>/N-doped carbon nanotubes/graphene (the best sputtering condition)) into the full cell and the achievement fraction (about 56%) of full discharge capacity for Al<sub>2</sub>O<sub>3</sub>/N-doped CNTs/graphene (the best sputtering condition) is higher than that (about 48%) for N-doped CNTs/graphene at a voltage higher than about 0.4 V (see Figures 11(a) and

11(b)). Al<sub>2</sub>O<sub>3</sub>/N-doped CNTs/graphene (the best sputtering condition) possessed better cyclic stability of discharge capacity and higher initial coulombic efficiency (79.8%) in comparison with N-doped CNTs/graphene (initial coulombic efficiency: 74.3%) (see Figures 11(a) and 11(b)) for the full cell since Al<sub>2</sub>O<sub>3</sub> improved bonding of SEI with carbon and reduced SEI formation during predischarging [7, 9]. So, the full cell for Al<sub>2</sub>O<sub>3</sub>/N-doped CNTs/graphene is a little higher potential for the benefit of merchantable lithium-ion batteries.

Figure 12 shows the effects of Al<sub>2</sub>O<sub>3</sub>/N-doped CNTs/graphene (the best sputtering condition), N-doped CNTs/graphene, and different charge-discharge cycles on the charge specific capacity (0.1 C) for the coin cell. The charge specific capacity fading for Al<sub>2</sub>O<sub>3</sub>/N-doped CNTs/graphene is a little smaller than that for N-doped CNTs/graphene (see Figure 12) which also is verified by the discharge-charge profiles of N-doped CNTs/graphene and Al<sub>2</sub>O<sub>3</sub>/N-doped CNTs/graphene (the best sputtering condition) (see Figures 9(a) and 9(b)). Because Al<sub>2</sub>O<sub>3</sub> improved bonding of SEI with carbon and then stabilized the electrode [7, 9], Al<sub>2</sub>O<sub>3</sub>/N-doped CNTs/graphene possessed a little better cycling performance (charge specific capacity only decreased 2.6% from the 1<sup>st</sup> cycle to the 20<sup>th</sup> cycle in Figure 12) compared with N-doped CNTs/graphene (charge specific capacity decreased 5.7% from the 1<sup>st</sup> cycle to the 19<sup>th</sup> cycle in Figure 12). Furthermore, Figure 13 shows the effects of different charge-discharge cycles on the coulombic efficiency of Al<sub>2</sub>O<sub>3</sub>/N-doped CNTs/graphene (the best sputtering condition) for the coin cell. Al<sub>2</sub>O<sub>3</sub>/N-doped CNTs/graphene possessed higher initial coulombic efficiency (81.44%) (see

Figure 13) in comparison with the N-doped CNTs/graphene composite (initial coulombic efficiency: 75.02%) [2] for the coin cell because  $\text{Al}_2\text{O}_3$  reduced SEI formation during pre-discharging [7, 9]. The more the cycle number, the more the stable SEI film, then the smaller the differences of the coulombic efficiency between cycles (see Figure 13). Moreover, since a uniform  $\text{Al}_2\text{O}_3$  coating layer with proper thickness could act as a preformed SEI to reduce regeneration of SEI (lithium-ion consumption) as well as then produce less SEI fragments during cycling and improved bonding of SEI with carbon as well as then stabilized the electrode [7, 9],  $\text{Al}_2\text{O}_3$ /N-doped CNTs/graphene (the best sputtering condition) compared with N-doped CNTs/graphene exhibited better rate performance at relatively high current density (0.5 C-2 C) for the coin cell (see Figure 14) which is similar to the previous literature [8].

#### 4. Conclusions

The longer the time period in the range 10-30 min for 65 W of the power level, the higher the charge specific capacity (coil cell). However, the longer the time period in the range 30-50 min for 65 W of the power level, the lower the charge specific capacity (coil cell). Furthermore, at a voltage higher than about 0.4 V, the achievement fraction (about 56%) of full discharge capacity (lithium-ion battery) for  $\text{Al}_2\text{O}_3$ /N-doped CNTs/graphene (the best sputtering condition) is higher than that (about 48%) for N-doped CNTs/graphene. Moreover,  $\text{Al}_2\text{O}_3$ /N-doped CNTs/graphene (the best sputtering condition) compared with N-doped CNTs/graphene possessed better rate performance at relatively high current density (0.5 C-2 C) for the coin cell.

#### Data Availability

Data of Raman, discharge/charge, and CV are available.

#### Conflicts of Interest

The authors declare that they have no conflicts of interest.

#### Acknowledgments

Financial support by the Ministry of Science and Technology of the Republic of China (under grant no. MOST 109-2221-E-224-008) is gratefully acknowledged.

#### References

- [1] D. Miranda, C. M. Costa, and S. Lanceros-Mendez, "Lithium ion rechargeable batteries: state of the art and future needs of microscopic theoretical models and simulations," *Journal of Electroanalytical Chemistry*, vol. 739, pp. 97–110, 2015.
- [2] C. C. Lin and P. L. Chang, "Synthesis of carbon nanotube/graphene composites on Ni foam without additional catalysts by CVD and their nitrogen-plasma treatment for anode materials in lithium-ion batteries," *Electrochemistry*, vol. 86, no. 3, pp. 109–115, 2018.
- [3] Y. He, X. Yu, Y. Wang, H. Li, and X. Huang, "Alumina-coated patterned amorphous silicon as the anode for a lithium-ion battery with high coulombic efficiency," *Advanced Materials*, vol. 23, no. 42, pp. 4938–4941, 2011.
- [4] J. Cui, J. Yang, J. Man et al., "Porous Al/ $\text{Al}_2\text{O}_3$  two-phase nanonetwork to improve electrochemical properties of porous C/SiO<sub>2</sub> as anode for Li-ion batteries," *Electrochimica Acta*, vol. 300, pp. 470–481, 2019.
- [5] S. Zhu, J. Liu, and J. Sun, "Precise growth of  $\text{Al}_2\text{O}_3$ /SnO<sub>2</sub>/CNTs composites by a two-step atomic layer deposition and their application as an improved anode for lithium ion batteries," *Electrochimica Acta*, vol. 319, pp. 490–498, 2019.
- [6] Q. Wu, B. Qu, J. Tang et al., "An alumina-coated Fe<sub>3</sub>O<sub>4</sub>-reduced graphene oxide composite electrode as a stable anode for lithium-ion battery," *Electrochimica Acta*, vol. 156, pp. 147–153, 2015.
- [7] Y. Fan, G. Clavel, and N. Pinna, "Effect of passivating  $\text{Al}_2\text{O}_3$  thin films on MnO<sub>2</sub>/carbon nanotube composite lithium-ion battery anodes," *Journal of Nanoparticle Research*, vol. 20, no. 8, p. 216, 2018.
- [8] T. Feng, Y. Xu, Z. Zhang et al., "Low-cost  $\text{Al}_2\text{O}_3$  coating layer as a preformed SEI on natural graphite powder to improve coulombic efficiency and high-rate cycling stability of lithium-ion batteries," *ACS Applied Materials & Interfaces*, vol. 8, no. 10, pp. 6512–6519, 2016.
- [9] I. Lahiri, S. M. Oh, J. Y. Hwang et al., "Ultrathin alumina-coated carbon nanotubes as an anode for high capacity Li-ion batteries," *Journal of Materials Chemistry*, vol. 21, no. 35, article 13621, 2011.
- [10] L. Wang, L. Zhang, Q. Wang et al., "Long lifespan lithium metal anodes enabled by  $\text{Al}_2\text{O}_3$  sputter coating," *Energy Storage Materials*, vol. 10, pp. 16–23, 2018.
- [11] C. C. Lin, Y. L. Shen, and A. N. Wu, "The effects of power level/s/time periods for sputtering cobalt onto carbon nanotubes/graphene composites and cobalt annealed on the characteristics of anode materials for lithium-ion batteries," *Journal of Nanomaterials*, vol. 2018, Article ID 9489042, 11 pages, 2018.
- [12] C. C. Lin, A. N. Wu, and S. H. Jiang, "Carbon nanotubes/graphene composites treated by nitrogen-plasma and covered with porous cobalt oxide through galvanostatic electrodeposition as well as annealing for anode materials of lithium-ion batteries," *Electrochemistry*, vol. 88, no. 1, pp. 14–21, 2020.
- [13] S. Kumari and A. Khare, "Optical and structural characterization of pulsed laser deposited ruby thin films for temperature sensing application," *Applied Surface Science*, vol. 265, pp. 180–186, 2013.
- [14] Y. Liu, B. Cheng, K. K. Wang et al., "Study of Raman spectra for  $\gamma$ - $\text{Al}_2\text{O}_3$  models by using first-principles method," *Solid State Communications*, vol. 178, pp. 16–22, 2014.
- [15] X. M. Liu, Z. D. Huang, S. W. Oh et al., "Carbon nanotube (CNT)-based composites as electrode material for rechargeable Li-ion batteries: a review," *Composites Science and Technology*, vol. 72, no. 2, pp. 121–144, 2012.